Modelling the Visual Response to an OUReP Retinal Prosthesis with Photoelectric Dye Coupled to Polyethylene Film

Koichiro Yamashita[1], Prathima Sundaram[2], Tetsuya Uchida[*1], Toshihiko Matsuo[3] and Willy Wong[*2]

[1] Graduate School of Natural Science and Technology, Okayama University, 3-1-1 Tsushima-naka, Kita-ku, Okayama 700-8530, Japan
[2] Department of Electrical and Computer Engineering, University of Toronto, 40 St. George Street, Toronto, Ontario M5S 2E4, Canada
[3] Graduate School of Interdisciplinary Science and Engineering in Health Systems, Okayama University, 2-5-1 Shikata-cho, Kita-ku, Okayama 700-8558, Japan

E-mail: [1] tuchida@cc.okayama-u.ac.jp, [2] willy.wong@utoronto.ca

Received xxxxxx
Accepted for publication xxxxxx
Published xxxxxx

Abstract

Objective. Retinal prostheses have been developed to restore vision in blind patients suffering from diseases like retinitis pigmentosa. *Approach.* A new type of retinal prosthesis called the Okayama University-type Retinal Prosthesis (OUReP) was developed by chemically coupling photoelectric dyes to a polyethylene film surface. The prosthesis works by passively generating an electric potential when stimulated by light. However, the neurophysiological mechanism of how OUReP stimulates the degenerated retina is unknown. *Main results.* Here, we explore how the OUReP affects retinal tissues using a finite element model to solve for the potential inside the tissue and an active Hodgkin-Huxley model based on rat vision to predict the corresponding retinal bipolar response. *Significance.* We show that the OUReP is likely capable of eliciting responses in retinal bipolar cells necessary to generate vision under most ambient conditions.

Keywords: retinal prosthesis, photoelectric dye, boundary value problem, biophysical models of retinal cells

1. Introduction

The mammalian retina consists of a photoreceptor cell layer, a bipolar cell layer, and a ganglion cell layer among other types of connecting cells. The photoreceptor cell layer is the starting point of vision whereby light entering the eye is converted into a neuroelectrical signal. Retinitis pigmentosa causes the loss of the photoreceptor cell layer and can lead to blindness [1-3]. Retinal prostheses can provide electrical stimulation to the living retinal tissues in substitution of the photoreceptor cell layer and have been developed in part to treat retinitis pigmentosa (figure 1).

In USA, the Argus II retinal prosthesis system (Second Sight Medical Products, Sylmar, CA, USA) has been approved by the U.S. Food and Drug Administration (FDA) [4-6]. The Argus II retinal prosthesis divides a camera-captured image into 60 pixels and then stimulates retinal tissues by outputting an electrical current which corresponds to a grayscale tone for each pixel. There are 60 electrodes implanted in the epiretinal space. The Photovoltaic Retinal Implant (PRIMA) is a system similar to Argus II requiring an

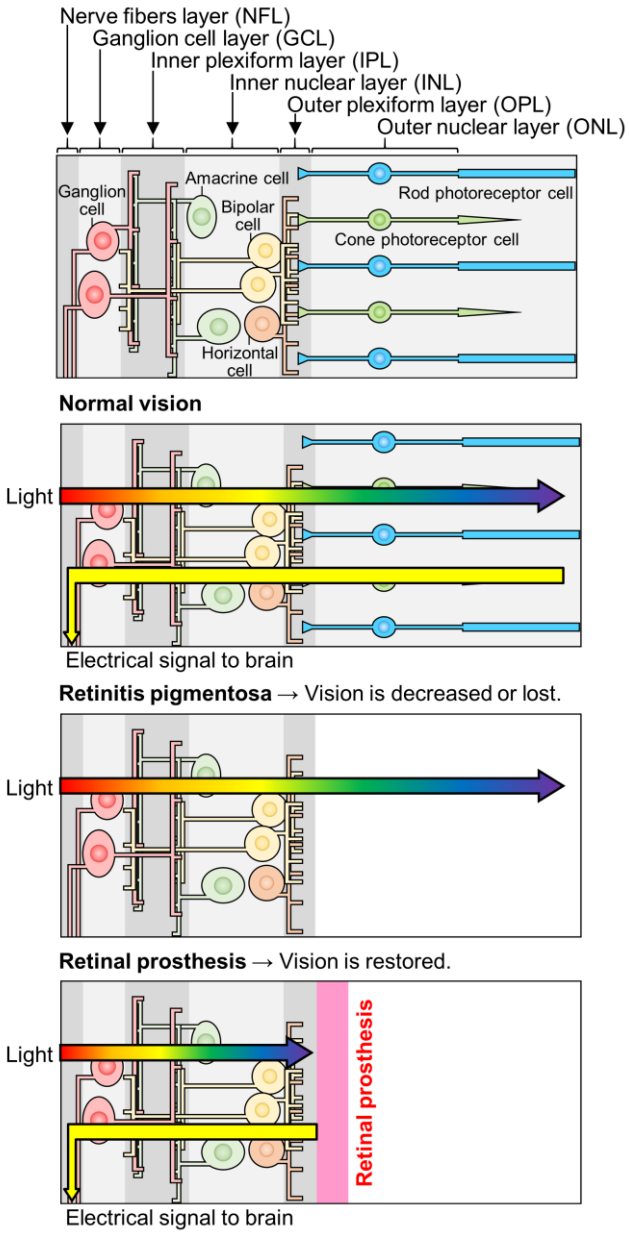

Figure 1. Spatial structure and organization of the mammalian retina. Of particular importance to light transduction are the photoreceptors, bipolar cells and ganglion cells. Photoreceptors are light sensitive and transduce light input into electrical signals. Retinitis pigmentosa is a disease whereby the photoreceptor layer is degenerated leading ultimately to blindness. Both an epi-retinal prosthesis (i.e. above the retina, adjacent to the ganglion layer) and a sub-retinal prosthesis (i.e. beneath the retina, adjacent to the photoreceptor/bipolar cells) can be used to restore vision.

external camera capture of the image, but with an electrode array implanted in the sub-retinal region [7]. The Retina Implant Alpha AMS (formerly Alpha IMS, Retina Implant AG, Aachen, Germany) has a sub-retinal multielectrode array of 1500 units, and each unit consists of a light sensitive photodiode, amplifier, and electrode [8-10]. The light picked up by the photodiode is amplified and a current is used to stimulate retinal cells. Recent studies have shown that the implant can last as long as 5 years [11] and provides improvements to the individual's visual function [12]. As with all electrode array systems, they require external power making it challenging to implant surgically and comes at a relatively high economical cost [13]. Similar implants have been proposed involving arrays implanted between the sclera and choroid with similar challenges [14-16]. Therefore, a retinal prosthesis that can improve upon existing solutions is highly desirable.

Photoelectric dye (2-[2-[4-(dibutylamino)phenyl]ethenyl]-3-carboxymethylbenzothiazolium bromide) is a π-conjugated compound that absorbs visible light. In other applications, this photoelectric dye has been utilized for dye-sensitized solar cells (DSC) [17-20]. The DSC consists of a dye-sensitized electrode whereby the photoelectric dye is chemically coupled to the titanium dioxide (TiO_2) surface, a transparent conductive glass, an external circuit, a cathode, and an electrolyte containing iodine. Since the oxidized dye is reduced by iodine in the electrolyte, the electrons in the dye molecules, when excited by absorbing light, can generate an electric current. To investigate their stability, DSC have been tested under various conditions including: 1,000 hr at 80 °C in darkness, 1000 hr at 60 °C at air mass (AM) 1.5, and as well as a combination of high temperature + light soaking. The DSC has shown good tolerance under a variety of conditions [18]. Additionally, aging tests conducted outdoors have demonstrated a lifespan of approximately 2.5 years [19].

In a previous study, the photoelectric dye was shown also to stimulate retinal neurons [21]. Therefore, the dye offers a promising solution as a key component to a retinal prosthetic device. However, the dye itself cannot be implanted directly in the retina due to its powdery state. Thus, a thin polyethylene (PE) film was selected as the substrate. A synthesis process was developed to couple the photoelectric dyes to the PE film surface, leading to the Okayama University-type retinal prosthesis (OUReP) [22-28]. The chemical structures and images showing the OUReP are shown in figure S1 of the supplementary materials.

Light absorption occurs in a part of the molecule known as the chromophore. By absorbing light, electrons in the molecule transition from the highest occupied molecular orbit (HOMO) to the lowest unoccupied molecular orbital (LUMO) and become an excited state [20]. Subsequently, dipoles are created, which in turn generate a dipole field. This is known as an exciton where the electron and electron hole are bounded by Coulombic forces. For the dye-sensitized solar cells, TiO_2 and conductive glass are used as substrates. For the retinal prosthesis, we have used instead a polyethylene film which acts as an insulator. Since the dye molecules are coupled to this film, the fields generated by the dye molecules will be aligned. This mechanism leads to the generation of an electrical potential on the OUReP surface which can be

measured using a scanning Kelvin probe (SKP) system [29-31]. The electrical potential is the source of visual stimulation in the OUReP.

There are several advantages to OUReP as a retinal prosthesis. First is that no external power source is required as the dye molecules work passively. Moreover, a minimally invasive injector has been developed to implant OUReP safely and easily into the sub-retinal space by vitreous surgery. This method has been shown to work in rabbit eyes [32, 33]. As for its safety and effectiveness, various tests for biocompatibility have now been conducted, and it has been demonstrated that the OUReP exhibits no toxicity. In an animal model study, the vision of retinal dystrophic rats (RCS rats) was restored by implanting the OUReP into blind rats [34-37]. The safety and feasibility of the implantation technique was further demonstrated in canine and rabbit eyes [38, 39]. More recently, OUReP has been implanted into monkey eyes with macular degeneration [40]. Visual evoked potentials (VEP) from the occipital cortex were measured to demonstrate visual stimulation. The amplitude of VEP, which was reduced due to macular degeneration, was recovered to normal levels one month after implantation and was maintained for five months post-operation demonstrating its effectiveness [41]. Finally, an in vitro evaluation technique was used to show the efficacy of OUReP using a multi-electrode array system and retinal tissue isolated from RCS rats [30] and rd1 mice [42]. For both studies, spikes were recorded from the array under various conditions of light stimulation, and the generation of spikes was dependent on the amount of dye coupled to the PE film surface. From this, we can conclude that a purely passive prosthesis like OUReP can not only facilitate vision, but also shows certain advantages over other types of retinal implant technology.

To further understand the efficacy of a visual prosthetic device, investigators have begun exploring the physiological response of visual cells to various implants. Studies are built upon existing mathematical models which are developed to model the physiological response of visual cells to external electrical potentials. Usui et al was one of the first to develop a mathematical model of the bipolar cell body by incorporating six ionic currents based on the response characteristics to voltage clamp experiments [43]. Usui's model includes a detailed model of the calcium currents. Experimental data from a variety of lower organisms were used to obtain model parameters for a Hodgkin-Huxley (HH)-type voltage dependent conductance equation. Moreover, Nishiyama et al went further to propose a network model between bipolar, photoreceptor, horizontal and amacrine cells [44]. Nishiyama's model includes the bipolar cell model of Usui et al. More recently, Benav et al have developed a model of the bipolar cell model which includes ten ionic currents [45]. Experimental results from rat bipolar cells were used to fit the HH equations for each current [46]. The model introduced a 3-D bipolar cell geometry and allows for different selections of ionic currents in each region of the cell [45, 47]. Benav's model includes a simplified form of the calcium model developed by Usui.

We follow the thrust of these studies by using physiological models of the visual cells to better clarify the interaction between the electrical potential generated by OUReP and the response in the visual pathway. Our aim is to create a model of a diseased retina, and then calculate the neural responses of the retinal cells under stimulation by OUReP. To accomplish this, we first measured the light-induced surface potential from the OUReP using the SKP system [29-31]. Next, a finite element method (FEM) was used to calculate the spatial distribution of the extracellular potential with OUReP in a diseased retina model [48]. From this model, we explored the sensitivity of the calculated potential to different choices of model parameters. In retinitis pigmentosa, the first layer of excitable cells are bipolar cells and thus, we focused our study on the electrical stimulation of bipolar cells with OUReP using models based on Benav et al and Usui et al.

2. Experimental section

2.1. Preparation of OUReP

We provide a short description of the preparation with the OUReP prosthesis. Further details can be found in earlier publications [29].

A thin polyethylene (PE) film was prepared from purified high-density polyethylene (HDPE) powder and the thickness was measured to be 30 ± 5 μm. The PE film was immersed into fuming nitric acid to introduce carboxyl moieties on the film surface. Next, the film was treated with the fuming nitric acid which reacted with ethylenediamine to change the carboxyl groups to amino groups. The photoelectric dyes (NK-5962, 503.5 g mol^{-1}, Hayashibara Inc., Okayama, Japan) were coupled to the amino moieties by dehydration condensation.

2.2. Light-induced surface electrical potential

The light-induced electrical potential on the OUReP was measured with the SKP system (SKP5050, KP Technology, Ltd., Highlands and Islands, UK) [29-31]. The entire measuring system was placed in a humidity-controlled box. Intensity and wavelength of light were controlled by a surface photovoltage spectroscopy (SPS) module (SPS040, KP Technology). The light was radiated by increasing the intensity from 0 to 3000 arbitrary unit (A.U.) in steps of 100 A.U. while the changes in surface electrical potential were recorded. Independently, we used a photometer to establish that a light intensity of 2500 A.U. corresponds approximately to 300 lux. This is the recommended level of light for studying in a classroom.

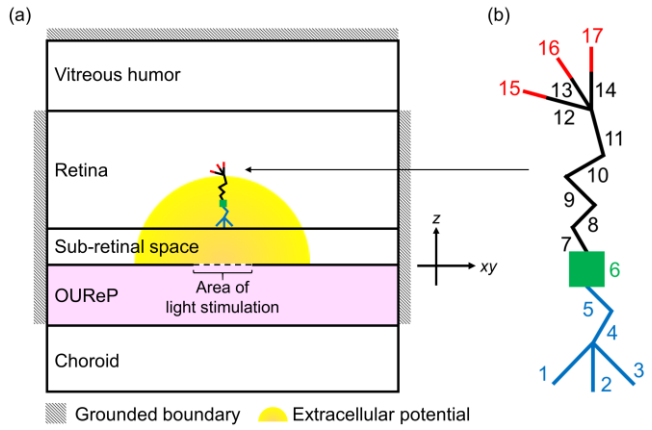

Figure 2. (a) A multi-layered retinal model used to calculate the spatial distribution of the electrical potential generated from the OUReP surface. (b) Morphology of the bipolar cell model and the number used to represent each assigned sections.

2.3. Model development

2.3.1. Modelling of multi-layered retinal model with OUReP

Figure 2(a) shows the multi-layered retinal model used in our calculations. It is a two-dimensional (2-D) axisymmetric model. The model consists of a vitreous humour layer, a retinal layer, sub-retinal space, OUReP (where the photoreceptors would ordinarily lie), and a choroid layer. Animal studies have indicated that the OUReP is not always in direct contact with the retinal layer [41]. This results in fluid-filled gaps that separate the OUReP and the tissue. In our model, these gaps were included as sub-retinal space. Table 1 shows the thickness and conductivity of each layer [29, 47, 49-51]. We used COMSOL Multiphysics (version 5.2a; COMSOL Inc., Burlington, MA, USA) for our calculations [48]. The vitreous humour was modelled as an infinite volume conductor and grounded at infinity. This allows the potential to fall to zero over the domain without having to model the full extent of the layer. The boundaries of the OUReP, sub-retinal space, and retinal layer were grounded in the manner shown in figure 2(a). The extracellular potential from the OUReP was implemented with the Electric Currents interface of the COMSOL AC/DC module. The spatial distribution of the extracellular potential in the multi-layered retinal model can be described through Maxwell's equations. The relevant equations are found in section S1 of the supplementary materials and solved using a finite element method in COMSOL.

2.3.2. Modelling of bipolar cell model

Most bipolar cells generate graded potentials, although spiking bipolar cells have also been identified recently [52, 53]. A graded response can be modelled by strictly passive RC-

Table 1. Thickness and conductivity values used in the multi-layered retinal model created in COMSOL Multiphysics.

	Thickness [μm]	Conductivity [S/m]
Vitreous Humor	Infinite	1.28 [50]
Retina	300 [47]	1.75 [47]
Sub-retinal Space	40 [49]	1.28 [50]
OUReP	30 [29]	1e-13 [51]
Choroid	407 [49]	0.037 [49]

circuits. However, active ion channels have also been found to play an important role. In this study, we will use a recently developed model, which includes ten ion channels [45, 47]. We refer to this as the "Benav model". Next, we provide a brief description of the included channels. In addition to the voltage-dependent sodium channel [54, 55], there are three types of potassium currents. A-type potassium (K) channel are responsible for repolarizing the membrane potential to rest potential in spiking cells [56]. The inward rectifying potassium (Kir) channels are believed to be the dominant determinant of the resting membrane potential and controls the excitability of the cell [57, 58], while calcium-activated potassium (KCa) channels are gated by calcium sensitive protein and respond to changes in calcium concentration and membrane potential [59, 60]. Hyperpolarization-activated cyclic nucleotide-gated (HCN) channels are permeable to both Na^+ and K^+ and are activated when the membrane potential becomes negative [61]. The kinetics of the HCN channel are slow relative to the other ion channels operating on a time scale of 100-1000 msec. The function of these channels is to bring the membrane back to the resting potential [45]. The Benav model includes the HCN1, HCN2, and HCN4 channels which are each encoded by different genes.

Concentrations in the intracellular and extracellular space can experience fluctuations due to influx and outflux of ions. However, ions are typically considered so numerous that the in/outflux does not change the actual level of concentration (i.e. they are treated as constant values). The only exception is the intracellular calcium (Ca) ion concentration, which is several orders of magnitude lower than the other ion concentrations. This means that the intracellular calcium concentration can increase significantly due to the inward flow of Ca^{2+}. There are two types of calcium channels that have been identified: the long-lasting (CaL) channel and the transient (CaT) channel. Depolarization causes Ca^{2+} to enter the cell resulting in a negative ionic current [43, 45, 47, 62]. Additionally, there is also the leakage (L) or non-gated channel.

Following [45], we have developed the bipolar cell model in seventeen sections. In this study, an active model with nine active ion channels was used. Several of the results were compared to a passive (leak-only) model to better understand the contribution of active channels to the response. Depending

Table 2. Morphology and active ion channels for each section of the bipolar cell model. The section numbers correspond to figure 2(b).

Section	Anatomical component	Ion channel	Radius [μm]	Length [μm]
1				3.5
2				4.8
3	Dendrite	Na, Leak	0.72	3.5
4				6.6
5				6.4
6	Soma	CaT, Kir, K, HCN1, HCN2, KCa, Leak	5.40	6.1
7				15.5
8				9.7
9				6.6
10	Axon	HCN4, Leak	0.76	12.6
11				10.8
12				13.1
13				6.4
14				6.3
15	Axon terminal	CaL, Na, HCN1, HCN2, HCN4, Leak	0.61	3.9
16				3.3
17				3.8

on the bipolar cell being considered, the type and variety of ion channels will vary [43, 45, 52]. The morphology and active ion channels assigned to each section are shown in table 2 and figure 2(b). Moreover, the total cell length in the *z*-dimension was taken to be 86.6 μm [45, 63]. Figure 3 shows the equivalent circuit model of the cell membrane. $I_{ion}(t)$ is the net ionic current density in each segment.

$$I_{ion}(t) = \sum_k I_k(t) + G_L(V_m - E_L) = \sum_k G_k(V_m - E_k) + G_L(V_m - E_L) \quad (1)$$

where I_k is the k^{th} ionic current (μAcm^{-2}), G_k the conductance (mScm^{-2}), V_m the membrane potential (mV), and E_k the equilibrium potential (mV). In the case where there is no external potential (V_{ext} = 0), the circuit can be solved using Kirchhoff's Law with the following equation

$$C_m \frac{dV_m}{dt} + I_{ion}(t) = \frac{1}{2\pi ar} \cdot \frac{\partial^2 V_m}{\partial x^2} \quad (2)$$

where C_m is the membrane capacitance (μFcm^{-2}), a is the radius of the segment (cm) and r, the axial resistance (kΩcm^{-1}). x is the spatial dimension in the axial direction. The value of axial resistance can vary along the length of neuron. However, we will assume it to be constant in our study. This model was implemented in an integrated Python environment employing the NEURON simulator [64]. The ability to manipulate the extracellular potential is not included in the default model. In order to change the external potential (V_{ext}), it was necessary to include an additional component [65].

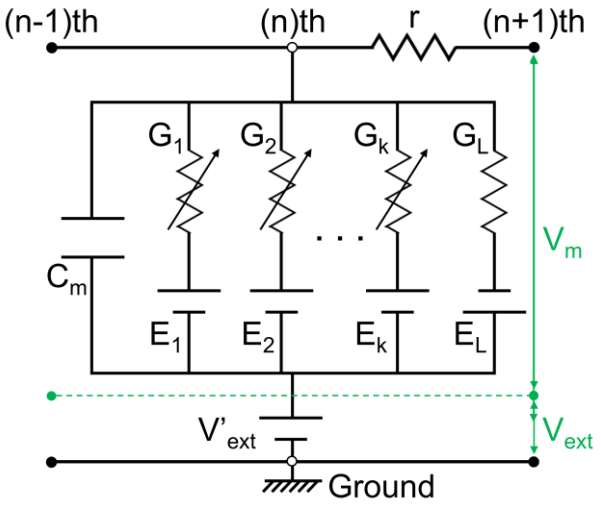

Figure 3. Equivalent electrical circuit model of cell membrane showing the active ion channels and leakage channel. k denotes the number of the ion channels in each section. The circuit model includes the ability to modify the external potential.

Details of the extracellular mechanism are described in figure S2 and table S1 of the supplementary materials. Since the membrane potential (V_m) is the difference between an intracellular potential (V_{int}) and an extracellular potential (V_{ext}), equation (3) can be written with V_{ext} shown explicitly [66].

$$C_m \frac{dV_m}{dt} + I_{ion}(t) = \frac{1}{2\pi ar}\left(\frac{\partial^2 V_m}{\partial x^2} + \frac{\partial^2 V_{ext}}{\partial x^2}\right) \quad (3)$$

Next, we explore the properties of this model by calculating the sensitivity of the response to various choices of parameters relevant to the design of the OUReP prosthesis.

2.3.3. Calculation of the extracellular potential induced by light absorption with OUReP and the corresponding bipolar cell response

The spatial distribution of the extracellular potential in the retinal layer from light stimulation of OUReP was first calculated with COMSOL and the resulting electric potential was extracted and imported into MATLAB (version R2017a; MathWorks Inc., Natick, MA, USA) [67]. The membrane potential along each section of the bipolar cell model was then calculated using the NEURON simulator. Unless otherwise noted, the responses were calculated under the conditions of an activation area of 200 μm diameter, an OUReP potential of 100 mV, which corresponds to a level of light equalling 300 lux, and a sub-retinal space of 40 μm which is typically observed in healthy vision [49]. For the retina, we choose a resistivity of 57 Ωcm which is similar in resistivity to 0.9% saline solution [45, 50, 68]. Since retinal fluid is similar to saline, we used a resistivity of 78 Ωcm when modelling the sub-retinal space [69]. To observe both the transient and

steady-state components of the response, the duration of the calculation was set to 100 msec.

2.4. Sensitivity analysis of bipolar cell response

2.4.1. Resistivity of retina and sub-retinal space

There exists a large discrepancy in the retinal resistivity values used in different published models. Some models use resistivity values as low as 57 Ωcm which is similar to 0.9% saline solution [45, 50, 68]. Other models use values as high as 10^4 Ωcm in accordance with measurements taken from rabbits and frogs [49, 70-72]. Additionally, the resistivity of sub-retinal space can also vary depending on the model [49, 73]. In some cases, the sub-retinal space is not explicitly modelled, therefore this layer is given the same resistivity as the other layers [47]. In order to evaluate the impact of resistivity, the retina and sub-retinal space were each modelled with a selection of resistivity values: 10^2 Ωcm, 10^3 Ωcm and, 10^4 Ωcm. Otherwise, the value of resistivity of the sub-retinal space was fixed to be at 78 Ωcm and the retina at 57 Ωcm.

2.4.2. Activation area of OUReP surface

The area of activation depends on the area of incident light. Here we calculate the distribution of extracellular potential and peak changes in membrane potential of the bipolar cell while changing the diameter of the activation area from 50 to 2000 µm. This corresponds to a visual stimulus spanning 0.3 to 13 degrees of retinal arc [41, 74].

2.4.3. Magnitude of potential from OUReP

The model was evaluated under the assumption that a small beam of light entered the eye activating the surface of the OUReP film. The surface potential generated by OUReP varies depending on the intensity of light. This relationship was measured with the SKP system and is shown in figure 4. The distributions of the extracellular potential along the *z*-axis and the subsequent bipolar cell responses were calculated while changing the potential at the surface of OUReP.

2.4.4. Position of bipolar cell relative to OUReP

As has been observed in [41], the prosthesis is not always in direct contact with the retinal layer. Therefore, the size of sub-retinal space can be a crucial factor in the bipolar cell response and can very well affect the clinical real-life use of OUReP as a visual prosthetic. Thus, the sub-retinal space was modelled with different thicknesses from 1-200 µm to analyse the impact of this gap. The end of the dendrite was fixed at the boundary between the sub-retinal space and the retinal layer. Since this turns out to be the most critical parameter in determining the activation of the bipolar cell, we decided to calculate the influence of position using both the ten-channel active model and the passive leak-only model.

Moreover, since the bipolar cell may not lie on the primary axis of the activation area of OUReP, we also simulated these conditions by moving the bipolar cell model from 0 µm to 500 µm "radially" along the *x*-axis. The thickness of sub-retinal space was set to 40 µm and the height of the end of dendrite was fixed at 40 µm. The distribution of the potential and peak changes in membrane potential of the bipolar cell were calculated. The responses were calculated under the conditions of an activation area of 200 µm and 50 µm diameter.

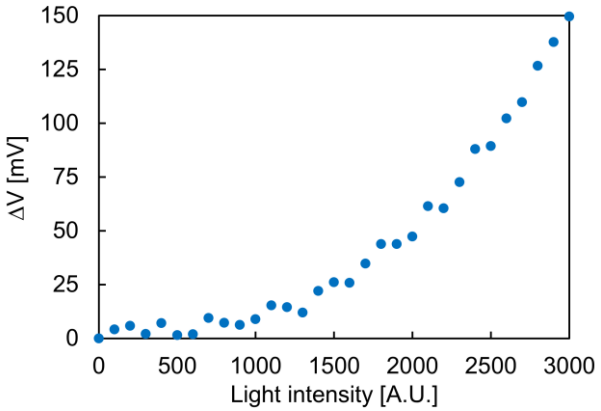

Figure 4. Light-induced surface electrical potentials measured from the OUReP using the scanning Kelvin probe system showing dependency on light intensity.

2.4.5. Cell morphology including length and diameter

To determine how the structure of the cell affects the membrane potential, the length and diameter of each section was modified and the peak changes in the membrane potential was calculated. First, the cell length was changed from 20% to 200% in 20% increments of the original cell length. Next, the impact of the diameter was investigated in the same manner. Similar to Section 2.4.4, the peak depolarization and hyperpolarization values for both the active and passive models were compared.

3. Results and Discussion

3.1. Photoresponsivity of OUReP

The light intensity dependence of OUReP is shown in figure 4. The surface potential is dependent on the incident light intensity and grows larger with increasing brightness. It has been previously shown that photoreceptor cells in the mouse exhibit a change in membrane potential on the order of tens of mV's in response to an external light stimulus [75]. Following the recommended light level for classrooms and normal office work, the light intensity was varied between 300-500 lux [76]. For such light levels, the recorded surface electrical potential was 89.3 mV at 2500 A.U. (300 lux) and 149.6 mV at 3000 A.U. (500 lux). Therefore, the change in potential at the OUReP surface is the same magnitude as that induced by the mouse rod photoreceptors. However, a change in potential

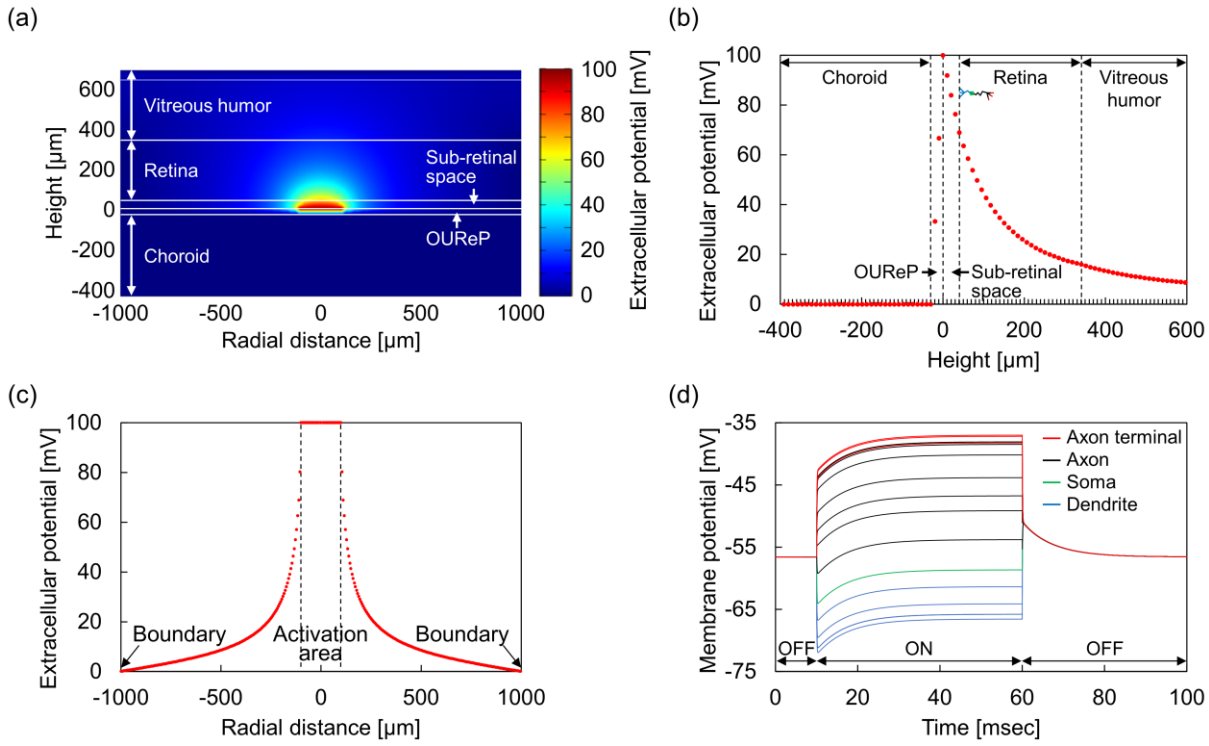

Figure 5. (a) Spatial distribution of the extracellular potential generated by activation of OUReP in a multi-layered retinal model. Area of light activation is centered at $z = 0$ µm in the xy-plane. Cross-sectional profile of the potential in (a) is shown in (b) and (c). (d) Temporal changes in membrane potential of the bipolar cell model induced by activation of OUReP from time 10-60 msec at different points along the cell.

does not, of course, provide a complete picture of how the visual system is stimulated.

3.2. Spatial distribution of the extracellular potential and bipolar cell response

The spatial distribution of the electric potential generated from the OUReP surface in the multi-layered retinal model is shown in figure 5(a). It is assumed that a spot of light with diameter 200 µm width and intensity 300 lux has irradiated the OUReP generating a subsequent potential of 100 mV on the film surface. The potential is symmetric about the axis of incident light. Due to the insulating effect from the PE film, the choroid layer is largely unaffected. The potential along the z-axis is shown in figure 5(b). As expected, the area closest to the activation site sees the highest potential. From here, the potential decreases rapidly in the vitreous humour. In the retinal layer, a maximum potential of 68.3 mV is recorded near the dendrite and a minimum potential of 38.8 mV at the axon terminal. By comparison, the spatial distribution of the potential in the choroid layer fell rapidly to zero. Thus, the choroid experiences little to no change in potential due to incident light. In figure 5(c), the variation of potential in the xy-plane is shown. The potential is approximately constant along the activation site from -100 to 100 µm, falling rapidly to zero as it approaches the boundaries consistent with the boundary conditions specified for the model. Finally, figure 5(d) shows the temporal change in the membrane potential of each section in the bipolar cell model induced by the potential at the OUReP film surface. The bipolar cell response reaches steady state by about 40 msec. Comparatively, bipolar cells in healthy vision reach steady state after 500 msec based on experimental results in rats [77, 78]. However, since these experimental results do not reflect isolated cells, it may be that single bipolar cells reach steady-state in shorter time periods of time.

3.3. Sensitivity analysis with bipolar cell response

3.3.1. Resistivity

The spatial distribution of the extracellular potential, profile of potential along the z-axis, and the peak change in membrane potential of the bipolar cell are found in figure 6. Figure 6(a) shows the result when 10^2 Ωcm, 10^3 Ωcm and 10^4 Ωcm are used as the resistivity of the retinal layer. A larger resistivity in the retinal layer results in a larger gradient of the potential. Calculating the maximum depolarization at the axon terminal, we found values of 22.5 mV, 26.9 mV, or 26.8 mV respectively. That is, the change in resistivity in the retinal layer had little impact on the bipolar cell response.

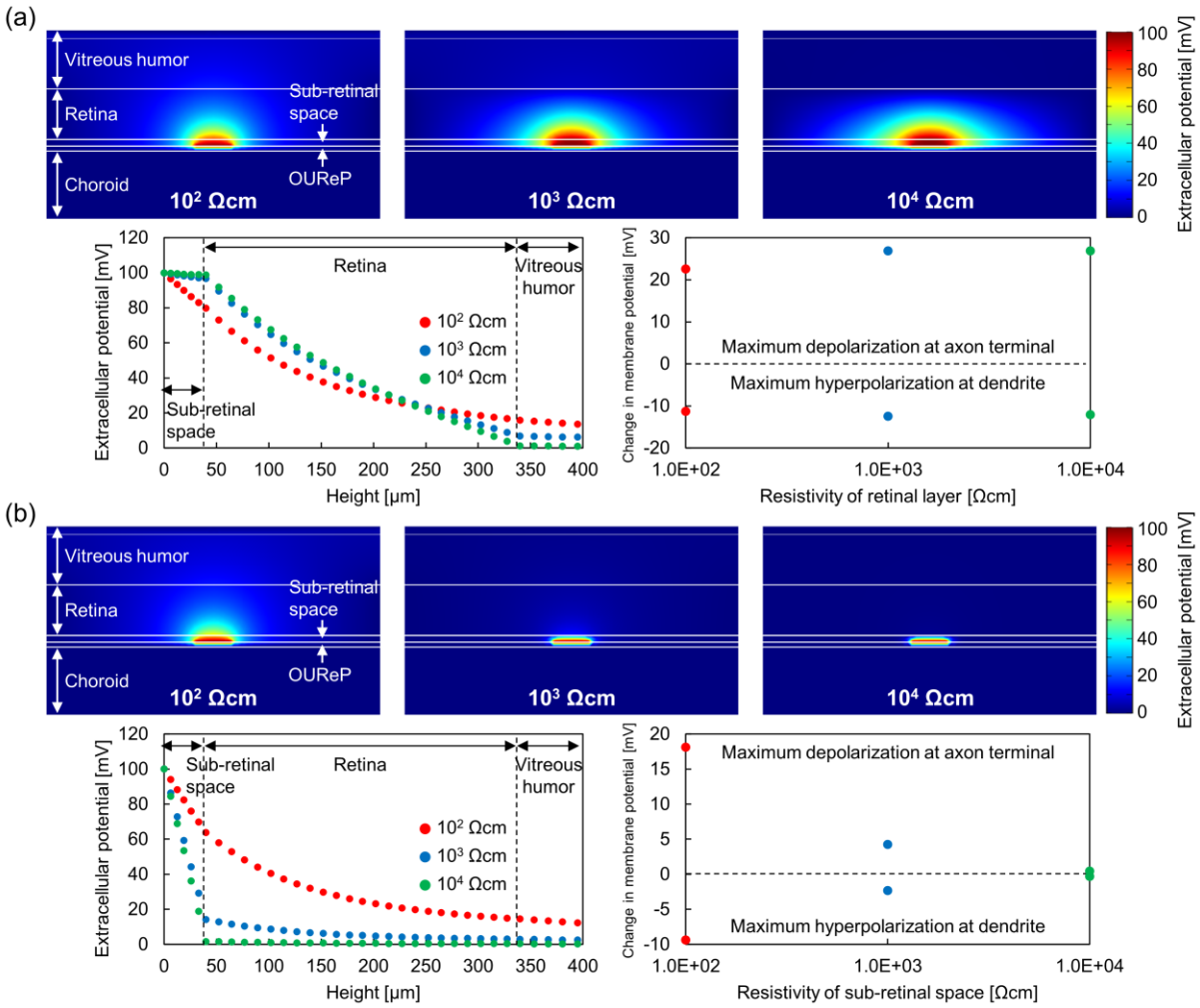

Figure 6. Influence of resistivity in the retinal and sub-retinal layer. (a) Extracellular potential when resistivity of 10^2 Ωcm, 10^3 Ωcm or, 10^4 Ωcm was used for the retinal layer. (b) Extracellular potential when resistivity of 10^2 Ωcm, 10^3 Ωcm or, 10^4 Ωcm was used for the sub-retinal space. Shown beneath both subfigures are the profiles of the potential along the *z*-axis and the maximum de/hyperpolarization values.

Figure 6(b) details the results when the resistivity of the sub-retinal space was changed to 10^2 Ωcm, 10^3 Ωcm and 10^4 Ωcm. The potential in the sub-retinal space decreased rapidly as the resistivity of sub-retinal space was increased. As a result, the maximum depolarization value at the axon terminal was 18.1 mV, 4.2 mV, or 0.4 mV, respectively. Therefore, as the resistivity of sub-retinal space was increased, both the potential in the retinal layer and the gradient of potential decreased resulting in a decreased bipolar cell response.

From these results, we can conclude that a change in resistivity in the retinal layer does not affect the bipolar cell response significantly. However, the choice in the resistivity of the sub-retinal space is crucial. A lower resistivity results in a much larger response. Since the sub-retinal layer is believed to have conductivity near that of saline, this is an important consideration in determining the OUReP induced visual response.

3.3.2. Area of activation on OUReP surface

Figure 7(a) shows the effect of the size of the activation area of light stimulation and figure 7(b) shows the same for the profile of the potential along the *z*-axis. The change in peak membrane potential is shown in figure 7(c). For small activation areas, the boundaries of the activation area cause the distribution of the potential to become distorted. The distortion falls directly over the location of the bipolar cell in the retinal layer. As the activation area increases, this effect becomes less pronounced. The depolarization is highest when the activation area is 200 μm in diameter. As the activation area becomes wider, the potential along the *z*-axis falls linearly as a consequence of the boundary conditions. Thus, the second derivative of the potential (i.e. the activating function [66]) will equal zero. The model predicts that OUReP will fail to stimulate the bipolar cells when large areas of the OUReP film

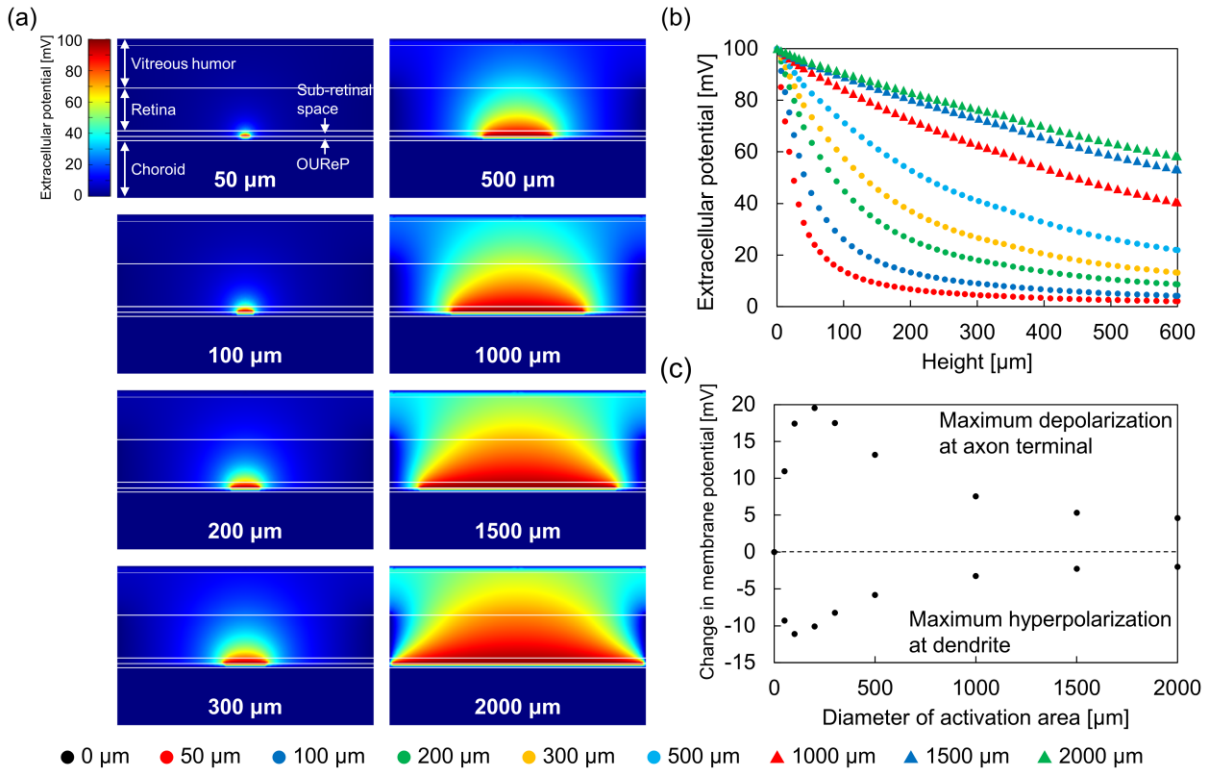

Figure 7. Influence of the activation area on extracellular potential. (a) Spatial distribution of extracellular potential. (b) Profile of potential along the *z*-axis. (c) Peak change in membrane potential in response to the potential. Activation area was varied from 50 to 2000 µm diameter.

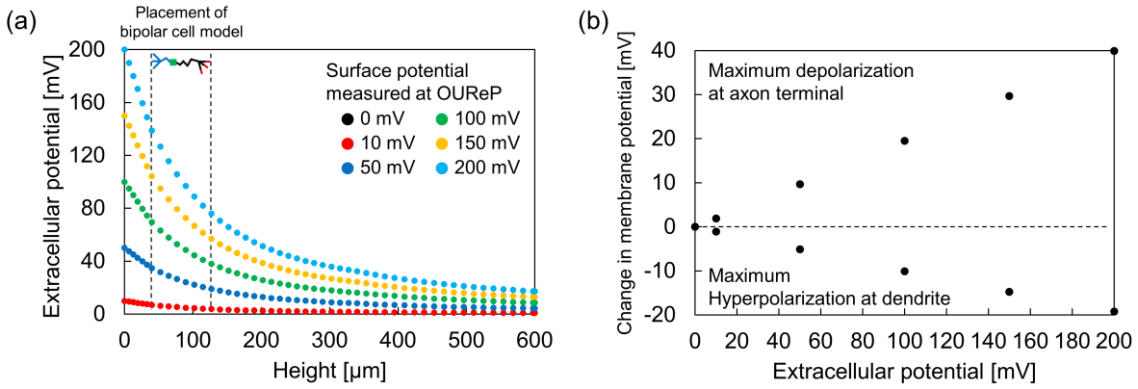

Figure 8. Effect of surface potential measured at OUReP on extracellular potential and peak response. (a) Profile of extracellular potential along the *z*-axis. (b) Peak change in bipolar cell response. Surface potential was varied from 0 to 200 mV.

are activated by uniform levels of light. A lack of bipolar response indicates little to no visual sensation for the user of the prosthesis.

This finding is based on the assumption that each layer of the multi-layered retinal model is entirely homogeneous, and that the incoming light is uniform. In reality, tissue morphology is inhomogeneous and the retinal cells do not lie parallel to the film. Thus, fluctuations in the electrical potential should lead to some activation of the bipolar cell although the resulting response is likely minimal.

3.3.3. Magnitude of extracellular potential from OUReP

Figure 8(a) shows the extracellular potential along the *z*-axis and figure 8(b) shows the changes in peak membrane potential. As the light intensity is increased, the value of the potential drops rapidly over the *z*-axis leading to an increase in the value of the activation function. As a result, the magnitude of the peak de/hyperpolarization value increases as the potential at $z = 0$ is increased. For context, the recommended light level for residential homes is 150 lux, classrooms 300 lux, offices 500

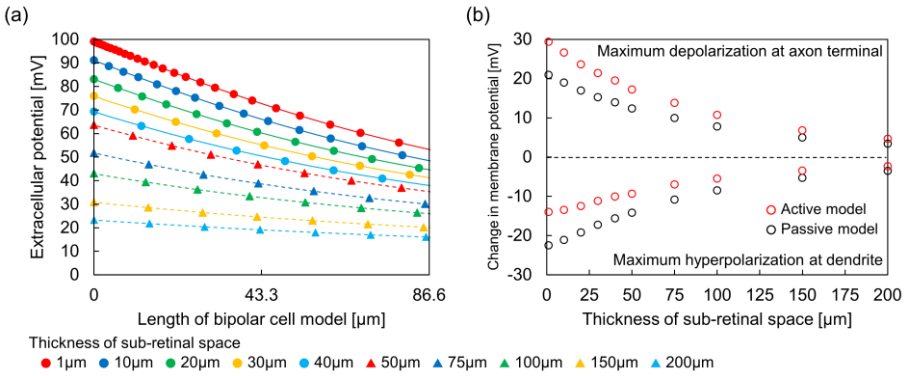

Figure 9. Influence of sub-retinal space between implant and bipolar cell layer. (a) Profile of the potential along the *z*-axis as a function of relative distance between implant and bipolar cell layer. (b) Peak de/hyperpolarization of response. Red dots are from active model, black dots, passive model.

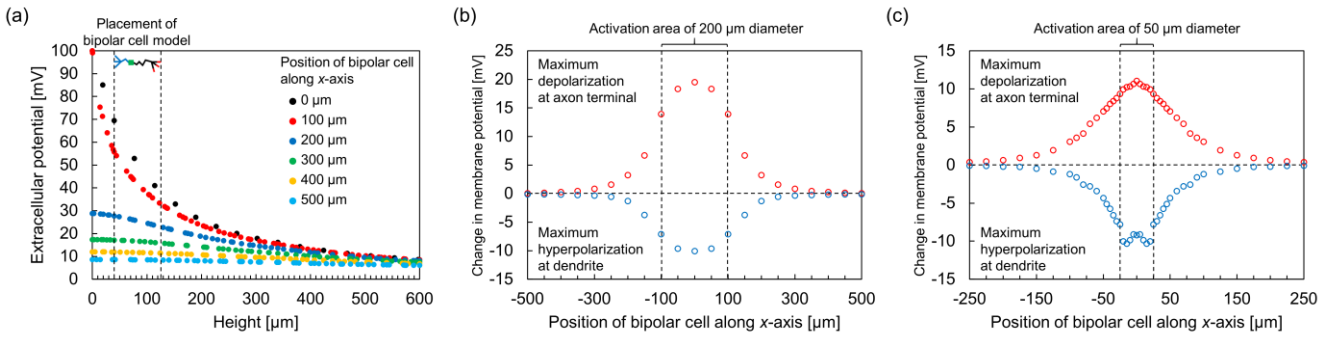

Figure 10. Influence of the relative position along the *x*-axis between center point of activation and bipolar cell. (a) Profile of potential as a function of relative distance along *x*-axis between center point of 200 μm diameter activation area and bipolar cell. Peak de/hyperpolarization response induced by activation area of (b) 200 μm diameter and (c) 50μm diameter.

lux, and mechanical workshops 1000 lux [76]. From the surface electrical potential measurements with the SKP system, the surface potential was found to be 100 mV at 300 lux, and 150 mV at 500 lux. The corresponding peak depolarization values of the bipolar cells were found to be 19.5 mV and 29.6 mV at these two levels of light illumination. Experimentally, it has been found that mammalian bipolar cells generate a change in depolarization around 20 mV in response to nominal levels of incident light [77]. This is one way of evaluating the efficacy of OUReP in facilitating vision.

Another way is to estimate the output of the retina which consists of spikes generated by retinal ganglion cells. The detailed connectivity between the bipolar and ganglion cells was explored in an earlier modelling study involving membrane depolarization, intracellular calcium concentration and subsequent neurotransmitter release [79]. The relationship between these three variables was found to be intricate, with too little depolarization to be insufficient to activate calcium channels at the bipolar terminals while too large a depolarization results in the prevention of synaptic transmission due to a reversal of calcium current. Nevertheless, a depolarization on order of 10 mV may fall in the right range to elicit vision. Future work can be carried out to extend the model of [79] to study synaptic transmission within the context of OUReP.

3.3.4. Position of OUReP relative to the bipolar cell

The photosensitive film is not always flush with the retinal tissue. Figure 9(a) shows the effects of the thickness of sub-retinal space on the response of the cells. When the gap between the bipolar cell and film is small, both a large potential and a large gradient is observed near the cell (due to the boundary condition at infinity). As a result, the change in membrane potential is the largest when the gap is the smallest. As the thickness is increased, both the potential and its gradient is decreased and a smaller response is observed. Thus, the exact placement of OUReP can greatly affect the magnitude of cellular response. To explore the contribution of active channels to the bipolar cell response, the de/hyperpolarization values for both the active and passive models were compared in figure 9(b). Note that '0 mV' is calculated with respect to the resting potential which was different for each model. The results show that for the active model, the depolarization at the axon terminal was increased

and the hyperpolarization at the dendrite decreased relative to the passive model. Therefore, the presence of the active channels contributes to greater activation. The efficacy of OURePP may depend on the role active channels have in controlling the response of the bipolar cells.

Figure 10(a) and 10(b) show the effect of the cell lying off-axis of stimulation. The diameter of activation area was set to 200 µm. The gradient of the potential drops dramatically outside the area of activation, resulting in a decrease in the magnitude for both hyperpolarization and depolarization. From this response, we can also provide a rough estimate of resolution of OURePP. By estimating the full-width at half-maximum from the bipolar depolarization response in figure 10(b), we observe that the response falls rapidly outside of the main area of activation. Carrying out a further calculation in figure 10(c) involving a smaller spot of light of 50 µm in diameter (approximately 0.25° in extent), the full-width at half-maximum is approximately 150 µm. Hence, we conclude that the resolution of OURePP is on order of 100 µm or less based on considerations of the bipolar response alone.

3.3.5. Influence of morphologies such as length and diameter

Figure 11(a) shows peak changes in membrane potential when the bipolar cell length was varied between 20 to 200 % of the original cell length. The maximum hyperpolarization value at the dendrite varies monotonically from -2.2 to -17.9 mV as the ratio of cell length was increased, while the depolarization varied monotonically from 5.2 to 24.1 mV. A difference in dendrite diameter between 20 to 200 % of original size results in only a change of 2.6 µm, with a difference in depolarization of only 0.04 mV. Similarly, for the axon, a change from 20 and 200 % of the original diameter results in a 2.2 µm difference, with depolarization changing by only 0.22 mV. These results are similar to the findings of Werginz et al where an increase/decrease of the bipolar cell's diameter did not result in a significant difference in response [47]. By a similar vein, since the intracellular resistance per length was kept constant, a soma of vastly differing size had a very different level of total resistance. However, this had only a minimal impact on the response similar to what was found in other studies [47, 80].

To investigate the contribution of active ion channels when length is changed, the de/hyperpolarization values were calculated for both the active and passive models. In figure 11(a), we see that the depolarization response is increased by the inclusion of active channels, but hyperpolarization is decreased. The discrepancy between the active and passive model increases as the change in length is increased. This indicates that different bipolar cells types (each with differing types of active channels) may see slightly different levels of response.

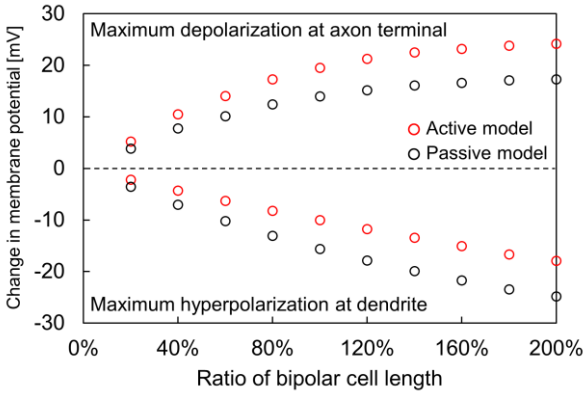

Figure 11. Influence of length of bipolar cell. Peak changes in membrane potential when ratio of the cell length was varied between 20 to 200% of original length. Red dots are from active model, black dots, passive model.

The length of bipolar cells can range from 40 to 90 µm [63]. From the above results, changing the diameter of bipolar cell had the smallest impact on the change in membrane potential. However, we also observe that longer bipolar cells receive greater activation than shorter bipolar cells. Under severe retinitis pigmentosa, degeneration of the bipolar cells is also observed resulting in a shortening of their length [81] which in turn will lead to smaller responses. Thus, vision will likely decreases due to cell degeneration even after implantation of OURePP.

3.4. Limitations in modelling and the implant

This study was undertaken to better understand the mechanism by which OURePP can help patients with retinitis pigmentosa restore their vision. Such an understanding is important because OURePP is fundamentally different from other types of retinal implants. However, limitations in our ability to model multiscale environments means that there are still gaps in our knowledge. For example, the issue of whether there is sufficient current to support the voltage imposed by OURePP cannot be well-answered at this time. For typical voltage-controlled stimulators, Merrill et al [82] set forth possible mechanisms for charge transfer in metal electrodes including both Faradaic and non-Faradaic sources. However, in the case of OURePP, we believe that no electrons are transferred from the implant to the tissue. Nevertheless, we believe that there is ample evidence showing that a visual response is induced experimentally via animal studies (e.g. Alamusi et al 2013 [34], Alamusi et al 2015 [35], Alamusi et al 2017 [36] and Matsuo et al 2018 [41]). The only question is how strong is this response and how long does it last. Clearly, this can only be answered definitively in the future when multiscale modelling continues to mature.

A key issue with most implanted stimulators is electrode encapsulation by fibrous tissue. However, OURePP does not have active electrode contacts and the implant consists of inert

materials that largely do not react with the body. In an earlier study with monkey eyes after six months of implantation, a small number of multinucleated giant cells were observed near the implanted film (Matsuo et al 2018 [41]). While the cells are not expected to have a large impact on the visual response (see results related to roughness and coarseness of the OUReP surface in section S3 of the supplementary materials), micrometre-level variations are difficult to quantify due to limitations in modelling methodology. As such, the effect of fibrous capsules on the retinal response can best be investigated during human trials.

4. Conclusions

The aim of this study was to explore the properties of the OUReP implant and how it affects mammalian bipolar cells in the diseased retina using biophysical models. First, we demonstrated that when stimulated with light levels typical of bright environments, OUReP induces a change in electrical potential that is of sufficient magnitude to induce a response in the retinal bipolar cell typically observed in mammalian vision. When studying the sensitivity of these results, the choice of resistivity of the retinal layer did not affect results substantially; however, changes in resistivity in the sub-retinal space had a much larger effect. Additionally, the size of the sub-retinal space is important: the smaller the gap between the implant and the cells, the larger the activation. Differences in the cell morphology did not result in large changes except for the total cell length. Since retinitis pigmentosa is a progressive disease, this would indicate that treatment can deteriorate over time due to the shortening in length of the cells. The results of this study can give further insight into improving the efficacy of sub-retinal implants of similar design as OUReP.

Acknowledgements

This work was supported by JSPS KAKENHI Grant Number JP19J13826.

References

[1] Loewenstein J I, Montezuma S R and Rizzo III JF 2004 Outer retinal degeneration: an electronic retinal prosthesis as a treatment strategy *Arch. Ophthalmol.* **122** 587-96

[2] Matsuo T and Morimoto N 2007 Visual acuity and perimacular retinal layers detected by optical coherence tomography in patients with retinitis pigmentosa *Br. J. Ophthalmol.* **91** 888-90

[3] Tamaki M and Matsuo T 2011 Erratum to: Optical coherence tomographic parameters as objective signs for visual acuity in patients with retinitis pigmentosa, future candidates for retinal prostheses *J. Artif. Organs* **14** 140-50

[4] Humayun M S, de Juan E, Jr. and Dagnelie G 2016 The Bionic Eye: A Quarter Century of Retinal Prosthesis Research and Development *Ophthalmology* **123** S89-97

[5] Humayun M S, Dorn J D, da Cruz L, Dagnelie G, Sahel J A, Stanga P E, Cideciyan A V, Duncan J L, Eliott D, Filley E, Ho A C, Santos A, Safran A B, Arditi A, Del Priore L V and Greenberg R J 2012 Interim Results from the International Trial of Second Sight's Visual Prosthesis *Ophthalmology* **119** 779-88

[6] da Cruz L, Dorn J D, Humayun M S, Dagnelie G, Handa J, Barale P O, Sahel J A, Stanga P E, Hafezi F, Safran A B, Salzmann J, Santos A, Birch D, Spencer R, Cideciyan A V, de Juan E, Duncan J L, Eliott D, Fawzi A, Olmos de Koo L C, Ho A C, Brown G, Haller J, Regillo C, Del Priore L V, Arditi A and Greenberg R J 2016 Five-year safety and performance results from the Argus II Retinal Prosthesis System clinical trial *Ophthalmology* **123** 2248-54

[7] Lorach H, Goetz G, Smith R, Lei X, Mandel Y, Kamins T, Mathieson K, Huie P, Harris J, Sher A and Palanker D 2015 Photovoltaic restoration of sight with high visual acuity *Nat. med.* **21** 476-82

[8] Stingl K, Bartz-Schmidt K U, Besch D, Braun A, Bruckmann A, Gekeler F, Greppmaier U, Hipp S, Hortdorfer G, Kernstock C, Koitschev A, Kusnyerik A, Sachs H, Schatz A, Sting K T, Peters T, Wilhelm B and Zrenner E, 2013 Artificial vision with wirelessly powered subretinal electronic implant alpha-IMS *Proc. R. Soc. B* **280** 20130077

[9] Stingl K, Bartz-Schmidt K U, Besch D, Chee C K, Cottriall C L, Gekeler F, Groppe M, Jackson T L, MacLaren R E, Koitschev A, Kusnyerik A, Neffendorf J, Nemeth J, Naeem M A N, Peters T, Ramsden J D, Sachs H, Simpson A, Singh M S, Wilhelm B, Wong D and Zrenner E 2015 Subretinal Visual Implant Alpha IMS – Clinical trial interim report *Vision Res.* **111** 149-60

[10] Stingl K, Schippert R, Bartz-Schmidt K U, Besch D, Cottriall C L, Edwards T L, Gekeler F, Greppmaier U, Kiel K, Koitschev A, Kühlewein L, MacLaren R E, Ramsden J D, Roider J, Rothermel A, Sachs H, Schröder G S, Tode J, Troelenberg N and Zrenner E 2017 Interim Results of a Multicenter Trial with the New Electronic Subretinal Implant Alpha AMS in 15 Patients Blind from Inherited Retinal Degenerations *Front. Neurosci*. **11** 445-55

[11] Gekeler K, Bartz-Schmidt K U, Sachs H, MacLaren R E, Stingl K, Zrenner E and Gekeler F 2018 Implantation, removal and replacement of subretinal electronic implants for restoration of vision in patients with retinitis pigmentosa *Curr. Opin. Ophthalmol.* **29** 239-47

[12] Edwards T L, Cottriall C L, Xue K, Simunovic M P, Ramsden J D, Zrenner E and MacLaren R E 2018 Assessment of the electronic retinal implant alpha AMS in restoring vision to blind patients with end-stage retinitis pigmentosa *Ophthalmology* **125** 432-43

[13] Second Sight Medical Products, Inc., Press Releases, November 6, 2018 [online] Available at: http://investors.secondsight.com/press-releases

[14] Abbott C J, Nayagam D A X, Luu C D, Epp S B, Williams R A, Salinas-LaRosa C M, Villalobos J, McGowan C, Shivdasani M N, Burns O, Leavens J, Yeoh J, Brandli A A, Thien P C, Zhou J, Feng H, Williams C E, Shepherd R K and Allen P J 2018 Safety studies for a 44-channel suprachoroidal retinal prosthesis: a chronic passive study *Investig. Ophthalmol. Vis. Sci.* **59** 1410-24

[15] Abbott C J, Nayagam D A X, Burns O, Feng H, McGowan C, Guymer R H, Williams C E, Allen P J and Luu C D 2019 Effect of chronic electrical stimulation with a fully implantable electrode on photoreceptor survival in a retinal degeneration model *Investig. Ophthalmol. Vis. Sci.* **60** 4992

[16] Fujikado T, Kamei M, Sakaguchi H, Kanda H, Endo T, Hirota M, Morimoto T, Nishida K, Kishima H, Terasawa Y, Oosawa K, Ozawa M and Nishida K 2016 One-Year Outcome of 49-Channel Suprachoroidal–Transretinal Stimulation Prosthesis in

Patients With Advanced Retinitis Pigmentosa *Investig. Ophthalmol. Vis. Sci.* **57** 6147-57
[17] Gratzel M 2005 Solar energy conversion by dye-sensitized photovoltaic cells *Inorg. Chem.* **44** 6841-51
[18] Sharma K, Sharma V and Sharma S S 2018 Dye-Sensitized Solar Cells: Fundamentals and Current Status *Nanoscale Res. Lett.* **13** 1-46
[19] Berginc M, Krasovec U O and Topic M 2014 Outdoor ageing of the dye-sensitized solar cell under different operation regimes *Sol. Energy Mater. Sol. Cells* **120** 491-9
[20] Hagberg D P, Marinado T, Karlsson K M, Nonomura K, Qin P, Boschloo G, Brinck T, Hagfeldt A and Sun L 2007 Tuning the HOMO and LUMO Energy Levels of Organic Chromophores for Dye Sensitized Solar Cells *J. Org. Chem.* **72** 9550-6
[21] Matsuo T 2003 A Simple Method for Screening Photoelectric Dyes towards Their Use for Retinal Prostheses *Acta Med. Okayama* **57** 257-60
[22] Tagawa T and Shimamura K 1980 Observation of the internal lamellar structure in polyethylene films by nitric acid treatment and SEM technique *J. Electron Microsc.* **28** 314-5
[23] Uchida T, Ishimaru S, Shimamura K, Uji A, Matsuo T and Ohtsuki H 2005 Immobilization of Photoelectric Dye on the Polyethylene FilmSurface *Mem. Fac. Eng. Okayama Univ.* **39** 16-20
[24] Uji A, Matsuo T, Ishimaru S, Kajiura A, Shimamura K, Ohtsuki H, Dan-oh Y and Suga S 2005 Photoelectric Dye-coupled Polyethylene Film as a Prototype of Retinal Prostheses *Aritif. Organs* **29** 53-7
[25] Uji A, Matsuo T, Uchida T, Shimamura K and Ohtsuki H 2006 Intracellular Calcium Response and Adhesiveness of Chick Embryonic Retinal Neurons to Photoelectric Dye-coupled Polyethylene Films as Prototypes of Retinal Prostheses *Artif. Organs* **30** 695-703
[26] Okamoto K, Matsuo T, Tamaki T, Uji A and Ohtsuki H 2008 Short-term biological safety of a photoelectric dye used as a component of retinal prostheses *J. Artif. Organs* **11** 45-51
[27] Tamaki T, Matsuo T, Hosoya O, Tsutsui K M, Uchida T, Okamoto K, Uji A and Ohtsuki H 2008 Glial reaction to photoelectric dye-based retinal prostheses implanted in the subretinal space of rats *J. Artif. Organs* **11** 38-44
[28] Matsuo T, Uchida T and Takarabe K 2009 Safety, efficacy, and quality control of a photoelectric dye-based retinal prosthesis (Okayama University-type retinal prosthesis) as a medical device *J. Artif. Organs* **12** 213-25
[29] Uchida T, Nitta M and Kanashima S 2015 Synthesis and Light-Induced Surface Potential Observation of Retinal Prosthesis Using Polyethylene Thin Films Immobilized with Photoelectric Dyes *J. Photopolym. Sci. Technol.* **28** 261-7
[30] Matsuo T, Sakurai M, Terada K, Uchida T, Yamashita K, Tanaka T and Takarabe K 2019 Photoelectric Dye-Coupled Polyethylene Film: Photoresponsive Properties Evaluated by Kelvin Probe and In Vitro Biological Response Detected in Dystrophic Retinal Tissue of Rats *Adv. Biomed. Eng.* **8** 137-44
[31] Baikie I D, Smith P J S, Porterfield D M and Estrup P J 1999 Multitip scanning bio-Kelvin probe *Rev. Sci. Instrum.* **70** 1842-50
[32] Matsuo T, Uchida T, Yamashita K, Matsuo C, Kawakami Y, Hitomi T, Taga K, Sanada T, Yamashita Y and Kuramoto K, 2018 Novel disposable injector (OUReP Injector) tested in experimental aphakic eyes of rabbits for subretinal implantation of Okayama University-type retinal prosthesis (OUReP) *Anim. Eye Res.* **37** 3-12
[33] Matsuo T, Matsuo C, Uchida T, Yamashita K, Tanaka T, Kawakami Y, Hitomi T, Taga K, Sanada T and Yamashita Y 2020 Curved-Tip Disposable Injector (OUReP Injector) to Insert Photoelectric Dye-Coupled Polyethylene Film (OUReP) as Retinal Prosthesis into Subretinal Space of Rabbit Eyes *Journal of Surgical Techniques and Procedures* **4** 1040-5
[34] Alamusi, Matsuo T, Hosoya O, Tsutsui K M and Uchida T 2013 Behavior tests and immunohistochemical retinal response analyses in RCS rats with subretinal implantation of Okayama University-type retinal prosthesis *J. Artif. Organs* **16** 343-51
[35] Alamusi, Matsuo T, Hosoya O, Tsutsui K M and Uchida T 2015 Vision maintenance and retinal apoptosis reduction in RCS rats with Okayama University-type retinal prosthesis (OURePTM) implantation *J. Artif. Organs* **18** 264-71
[36] Alamusi, Matsuo T, Hosoya O and Uchida T 2017 Visual evoked potential in RCS rats with Okayama University-type retinal prosthesis (OURePTM) implantation *J. Artif. Organs* **20** 158-65
[37] Matsuo T, Uchida T, Yamashita K, Takei S, Ido D, Fujiwara A, Iino M and Oguchi M 2019 Vision evaluation by functional observational battery, operant behavior test, and light/dark box test in retinal dystrophic RCS rats versus normal rats *Heliyon* **5** e01936-43
[38] Matsuo T, Uchida T, Nitta M, Yamashita K, Takei S, Ido D, Tanaka M, Oguchi M and Furukawa T 2017 Subretinal implantation of Okayama University-type retinal prosthesis (OUReP^{TM}) in canine eyes by vitrectomy *J. Vet. Med. Sci.* **79** 1939-46
[39] Matsuo T, Uchida T, Yamashita K, Takei S, Ido D, Tanaka M, Oguchi M and Furukawa T 2018 Visual evoked potential in rabbits' eyes with subretinal implantation by vitrectomy of Okayama University-type retinal prosthesis (OUReP^{TM}) *J. Vet. Med. Sci.* **80** 247-59
[40] Shirai H, Mandai M, Matsushita K, Kuwahara A, Yonemura S, Nakano T, Assawachananont J, Kimura T, Saito K, Terasaki H, Eiraku M, Sasai Y and Takahashi M 2015 Transplantation of human embryonic stem cell-derived retinal tissue in two primate models of retinal degeneration *PNAS* **113** E81-90
[41] Matsuo T, Uchida T, Sakurai J, Yamashita K, Matsuo C, Araki T, Yamashita Y and Kamikawa K 2018 Visual Evoked Potential Recovery by Subretinal Implantation of Photoelectric Dye-Coupled Thin Film Retinal Prosthesis in Monkey Eyes With Macular Degeneration *Artif. Organs* **42** E186-203
[42] Matsuo T, Terada K, Sakurai M, Liu S, Yamashita K and Uchida T 2020 Step-by-Step Procedure to Test Photoelectric Dye Coupled Polyethylene Film as Retinal Prosthesis to Induce Light-Evoked Spikes in Isolated Retinal Dystrophic Tissue of rd1 Mice *Clin. Surg.* **5** 2903-11
[43] Usui S, Ishihaiza A, Kamiyama Y and Ishii H 1996 Ionic current model of bipolar cells in the lower vertebrate retina *Vision Res.* **36** 4069-76
[44] Nishiyama S, Hosoki Y, Koike C and Amano A 2014 Reproducing retinal rod bipolar cell light response by mathematical model including neurotransmitter receptors *Annual International Conference of the IEEE Engineering in Medicine and Biology Society* **2014** 6116-9
[45] Benav H 2012 Modeling effects of extracellular stimulation on retinal bipolar cells *Ph.D. Thesis* Eberhard Karls Universitaet Tuebingen
[46] Hodgkin A L and Huxley A F 1952 A quantitative description of membrane current and its application to conduction and excitation in nerve *J. Physiol.* **117** 500-44
[47] Werginz P, Benav H, Zrenner E and Rattay F 2015 Modeling the response of ON and OFF retinal bipolar cells during electric stimulation *Vision Res.* **111** 170-81

[48] COMSOL AB 2010 *COMSOL Multiphysics User's Guide* **Version 4.0a**
[49] Sui X, Huang Y, Feng F, Huang C, Chan L L H and Wang G 2015 3D Finite Element Modeling of Epiretinal Stimulation: Impact of Prosthetic Electrode Size and Distance from the Retina *Int. J. Artif. Organs* **38** 277-87
[50] Geddes L A and Baker L E 1967 The specific resistance of biological material-A compendium of data for the biomedical engineer and physiologist *Med. Biol. Eng.* **5** 271-93
[51] Wypych G 2016 *Handbook of Polymers* 2nd edn
[52] Rattay F, Bassereh H, Fellner A 2017 Impact of Electrode Position on the Elicitation of Sodium Spikes in Retinal Bipolar Cells *Sci. Rep.* **7** 1-12
[53] Puthussery T, Venkataramani S, Gayet-Primo J, Smith R G, Taylor W R 2013 Nav1.1 Channels in Axon Initial Segments of Bipolar Cells Augment Input to Magnocellular Visual Pathways in the Primate Retina *J. Neurosci.* **33** 16045-59
[54] Cui J and Pan Z H 2008 Two Types of Cone Bipolar Cells Express Voltage-Gated Na^+ Channels in the Rat Retina *Vis. Neurosci.* **25** 635-45
[55] Ichinose T, Shields C R and Lukasiewicz P D 2005 Sodium Channels in Transient Retinal Bipolar Cells Enhance Visual Responses in Ganglion Cells *J. Neurosci.* **25** 1856-65
[56] Mao B Q, Macleish P R and Victor J D 2002 Relation Between Potassium-Channel Kinetics and the Intrinsic Dynamics in Isolated Retinal Bipolar Cells *J. Comput. Neurosci.* **12** 147-63
[57] Isomoto S, Kondo C and Kurachi Y 1997 Inwardly Rectifying Potassium Channels: Their Molecular Heterogeneity and Function *Japanese J. Physiol.* **47** 11-39
[58] Ma Y P, Cui J, Hu H J and Pan Z H 2003 Mammalian Retinal Bipolar Cells Express Inwardly Rectifying K^+ Currents (I Kir) With a Different Distribution Than That of I h *J. Neurophysiol.* **90** 3479-89
[59] Vergara C, Latorre R, Marrion N V and Adelman J P 1998 Calcium-activated potassium channels *Curr. Opin. Neurobiol.* **8** 321-9
[60] Wang G Y, Robinson D W and Chalupa L M 1998 Calcium-Activated Potassium Conductances in Retinal Ganglion Cells of the Ferret *J. Neurophysiol.* **79** 151-8
[61] Yang Q, Kuzyk P, Antonov I, Bostwick C J, Kohn A B, Moroz L L and Hawkins R D 2015 Hyperpolarization-activated, cyclic nucleotide-gated cation channels in Aplysia: Contribution to classical conditioning *PNAS* **112** 16030-5
[62] Pan Z H 2000 Differential Expression of High- and Two Types of Low-Voltage–Activated Calcium Currents in Rod and Cone Bipolar Cells of the Rat Retina *J. Neurophysiol*. **83** 513-27
[63] Euler T, Wässle H 1995 Immunocytochemical identification of cone bipolar cells in the rat retina *J. Comp. Neurol.* **361** 461-78
[64] Hines M L and Carnevale N T 1997 The NEURON Simulation Environment *Neural Comput.* **9** 1179-1209
[65] Appukuttan S, Brain K L and Manchanda R 2017 Modeling extracellular fields for a three-dimensional network of cells using NEURON *J. Neurosci. Methods* **290** 27-38
[66] Rattay F 1989 Analysis of models for extracellular fiber stimulation *IEEE Trans. Biomed. Eng.* **36** 676-82
[67] The MathWorks Inc., MATLAB version 9.2.0.538062 (R2017a), 2017 [online] Available at: http://www.mathworks.com
[68] Doslak M J, Plonsey R and Thomas C W 1980 The Effects of Variations of the Conducting Media Inhomogeneities on the Electroretinogram *IEEE. Trans. Biomed. Eng.* **BME-27** 88-94
[69] Greenberg R J, Velte T J, Humayun M S, Scarlatis G N and De Juan E 1999 A computational model of electrical stimulation of the retinal ganglion cell *IEEE. Trans. Biomed. Eng.* **46** 505-14
[70] Cao X, Sui X, Lyu Q, Li L and Chai X 2015 Effects of different three-dimensional electrodes on epiretinal electrical stimulation by modeling analysis *J. Neuroeng. Rehabil.* **12** 1-15
[71] Kasi H, Hasenkamp W, Cosendai G, Bertsch A and Renaud P 2011 Simulation of epiretinal prostheses - evaluation of geometrical factors affecting stimulation thresholds *J. Neuroeng. Rehabil.* **8** 1-10
[72] Karwoski C J and Xu X 1999 Current source-density analysis of light-evoked field potentials in rabbit retina *Vis. Neurosci.* **16** 369-77
[73] Joarder S A, Abramian M, Suaning G J, Lovell N H and Dokos S 2011 A continuum model of retinal electrical stimulation *J. Neural Eng.* **8** 066006
[74] Atsumi I, Kurata M and Sakaki H 2013 Comparative study on ocular anatomical features among rabbits, beagle dogs and cynomolgus monkeys *Anim. Eye Res.* **32** 35-41
[75] Okawa H, Sampath A P, Laughlin S B and Fain G L 2008 ATP Consumption by Mammalian Rod Photoreceptors in Darkness and in Light *Curr. Biol.* **18** 1917-21
[76] Engineering ToolBox 2004 *Illuminance - Recommended Light Level* [online] Available at: https://www.engineeringtoolbox.com/light-level-rooms-d_708.html [Accessed 28th July 2020]
[77] Euler T and Masland R H 2000 Light-Evoked Responses of Bipolar Cells in a Mammalian Retina *J. Neurophysiol.* **83** 1817-29
[78] Berntson A and Taylor W R 2000 Response characteristics and receptive field widths of on-bipolar cells in the mouse retina *J. Physiol.* **524** 879-89
[79] Werginz P and Rattay F 2016 The impact of calcium current reversal on neurotransmitter release in the electrically stimulated retina *J. Neural Eng.* **13** 046013
[80] Sundaram P 2020 Response of Retinal Ganglion Cells to Electrical Stimulation: From Prosthesis to "Seeing" *MSc Thesis* University of Toronto
[81] Humayun M S, Prince M, de Juan E, Jr., Barron Y, Moskowitz M, Klock I B and Milam A H 1999 Morphometric analysis of the extramacular retina from postmortem eyes with retinitis pigmentosa *Investig. Ophthalmol. Vis. Sci.* **40** 143-8
[82] Merrill D R, Bikson M, Jefferys J G R 2005 Electrical stimulation of excitable tissue: design of efficacious and safe protocols *J. Neurosci. Methods* **141** 171-98